SIAM J. APPL. MATH.
Vol. 67, No. 3, pp. 893–913
© 2007 Society for Industrial and Applied Mathematics

D-BAR METHOD FOR ELECTRICAL IMPEDANCE TOMOGRAPHY WITH DISCONTINUOUS CONDUCTIVITIES*

KIM KNUDSEN†, MATTI LASSAS‡, JENNIFER L. MUELLER§, AND SAMULI SILTANEN¶

Abstract. The effects of truncating the (approximate) scattering transform in the D-bar reconstruction method for two-dimensional electrical impedance tomography are studied. The method is based on the uniqueness proof of Nachman [*Ann. of Math.* (2), 143 (1996), pp. 71–96] that applies to twice differentiable conductivities. However, the reconstruction algorithm has been successfully applied to experimental data, which can be characterized as piecewise smooth conductivities. The truncation is shown to stabilize the method against measurement noise and to have a smoothing effect on the reconstructed conductivity. Thus the truncation can be interpreted as regularization of the D-bar method. Numerical reconstructions are presented demonstrating that features of discontinuous high contrast conductivities can be recovered using the D-bar method. Further, a new connection between Calderón's linearization method and the D-bar method is established, and the two methods are compared numerically and analytically.

Key words. inverse conductivity problem, electrical impedance tomography, exponentially growing solution, Faddeev's Green's function

AMS subject classifications. 35R30, 65N21, 92C55

DOI. 10.1137/060656930

1. Introduction.

The two-dimensional (2-D) inverse conductivity problem is to determine and reconstruct an unknown conductivity distribution γ in an open, bounded, and smooth domain $\Omega \subset \mathbb{R}^2$ from voltage-to-current measurements on the boundary $\partial\Omega$. We assume that there is a $C > 0$ such that

$$C^{-1} < \gamma(x) < C, \quad x \in \Omega. \tag{1}$$

The boundary measurements are modeled by the Dirichlet-to-Neumann (DN) map

$$\Lambda_\gamma f = \gamma \frac{\partial u}{\partial \nu}\Big|_{\partial\Omega},$$

where u is the solution to the generalized Laplace equation

$$\nabla \cdot \gamma \nabla u = 0 \quad \text{in } \Omega, \quad u|_{\partial\Omega} = f. \tag{2}$$

Mathematically, the problem is to show that the map $\gamma \mapsto \Lambda_\gamma$ is injective and find an algorithm for the inversion of the map. Physically, u is the electric potential in Ω, and Λ_γ represents knowledge of the current flux through $\partial\Omega$ resulting from the voltage distribution f applied on $\partial\Omega$.

*Received by the editors April 10, 2006; accepted for publication (in revised form) December 28, 2006; published electronically April 13, 2007.
http://www.siam.org/journals/siap/67-3/65693.html

†Department of Mathematical Sciences, Aalborg University, Fredrik Bajers Vej 7G, DK-9220 Aalborg Ø, Denmark (kim@math.aau.dk). This author was supported by the Carlsberg Foundation.
‡Institute of Mathematics, Helsinki University of Technology, P.O. Box 1100, 02015 TKK, Finland (matti.lassas@hut.fi). This author was supported by the Academy of Finland.
§Department of Mathematics, Colorado State University, Fort Collins, CO 80523 (mueller@math.colostate.edu). This author was supported by the National Science Foundation under grant 0513509.
¶Institute of Mathematics, Tampere University of Technology, P.O. Box 553, 33101 Tampere, Finland (samuli.siltanen@tut.fi). This author was supported by the Academy of Finland.

The inverse conductivity problem has applications in subsurface flow monitoring and remediation [30, 31], underground contaminant detection [10, 17], geophysics [9, 27], nondestructive evaluation [11, 36, 39, 37], and a medical imaging technique known as electrical impedance tomography (EIT) (see [8, 5] for a review article on EIT). Conductivity distributions appearing in applications are typically piecewise continuous. This is the case, for example, in medical EIT, since various tissues in the body have different conductivities, and there are discontinuities at organ boundaries. Here we consider 2-D reconstructions. These can be used to image cross-sections of a three-dimensional (3-D) region, such as a patient's torso. In the case of patients receiving mechanical ventilation, for example, 2-D cross-sections are useful for obtaining regional ventilation information in the lungs, which is valuable for setting and controlling the airflow and pressure settings on the ventilator [34, 1]. Real-time imaging of cross-sectional lung activity can also be used for diagnostic purposes, such as detecting a lung collapse, a pulmonary embolism, pulmonary edema, or a pneumothorax.

Let us briefly outline the history of D-bar solution methods for EIT. Recently, Astala and Päivärinta [2] showed that knowledge of the DN map uniquely determines the conductivity $\gamma(x) \in L^\infty(\Omega)$, $0 < c \le \gamma$. This result has been generalized to anisotropic conductivities in [3]. In this work, we will refer to the 2-D uniqueness result by Nachman [25] for $\gamma \in W^{2,p}(\Omega)$, $p > 1$, and by Brown and Uhlmann [6] for $\gamma \in W^{1,p}(\Omega)$, $p > 2$. The proof in [25] is constructive; that is, it outlines a direct method for reconstructing the conductivity γ from knowledge of Λ_γ. This method was realized as a numerical algorithm for C^2 conductivities in [29, 24, 15]. The uniqueness result of Brown and Uhlmann in [6] was formulated as a reconstruction algorithm in [20], which has been implemented in [18, 19]. There are many similarities between the two methods. In fact, it was shown in [18] using the Brown–Uhlmann approach that the reconstruction method of Nachman [25] can be extended to the class of conductivities $\gamma \in W^{1+\epsilon,p}(\Omega)$, $p > 2$, $\epsilon > 0$. We refer the reader to [24, 5, 38] for discussions of uniqueness results for γ in other spaces and $\Omega \subset \mathbb{R}^n$, $n \ge 2$.

Nachman's D-bar approach in [25] is based on the evaluation of the scattering transform $\mathbf{t}(k)$ by the formula

$$\mathbf{t}(k) = \int_{\partial\Omega} e^{i\overline{k}\bar{x}}(\Lambda_\gamma - \Lambda_1)\psi(\cdot,k)d\sigma(x), \quad k \in \mathbb{C},\ x = x_1 + ix_2, \tag{3}$$

where Λ_1 denotes the DN map corresponding to the homogeneous conductivity 1. Then γ can be recovered by solving a D-bar equation containing $\mathbf{t}(k)$. The functions $\psi(\cdot,k)$ in (3) are traces of certain exponentially growing solutions to (2), i.e., solutions that behave like e^{ikx} asymptotically as either $|x|$ or $|k|$ tends to infinity. These traces can, in principle, be found by solving a particular boundary integral equation. However, as solving such an equation is quite sensitive to measurement noise, the following approximation to $\mathbf{t}(k)$ was introduced in [29]:

$$\mathbf{t}^{\exp}(k) = \int_{\partial\Omega} e^{i\overline{k}\bar{x}}(\Lambda_\gamma - \Lambda_1)e^{ikx}d\sigma(x). \tag{4}$$

This approximation can be viewed as a linearizing assumption, since the approximation $\psi|_{\partial\Omega} \approx e^{ikx}$ is used instead of solving for ψ on the boundary using the nonlinear equation (7).

Formula (4) allows the evaluation of $\mathbf{t}^{\exp}(k)$ for L^∞ conductivities, and the D-bar method is found to be effective even when the conductivity does not satisfy the assumptions of the original reconstruction theorem. In [15], quite accurate reconstructions are computed from experimental data collected on a phantom chest consisting

of agar heart and lungs in a saline-filled tank. They are the first reconstructions using the D-bar method on a discontinuous conductivity and on measured data. In [16], the D-bar algorithm with a differencing $\mathbf{t}^{\exp}$ approximation is used to reconstruct conductivity changes in a human chest, particularly pulmonary perfusion.

Our aim is to better understand the reconstruction of realistic conductivities from noisy EIT data using the D-bar method by studying its application to piecewise smooth conductivities. Section 2 gives necessary background on the method and its variants. In section 3, we prove that reconstructions from any truncated scattering data are smooth. In section 4, we show that the reconstructions from noisy data using truncated $\mathbf{t}^{\exp}$ are stable. We remark that previous work [23, 4] shows that the exact reconstruction algorithm is stable in a restricted sense, i.e., as a map defined on the range of the forward operator $\Lambda\colon \gamma \mapsto \Lambda_\gamma$. In contrast, we show that the approximate reconstruction is continuously defined on the entire data space $\mathcal{L}(H^{1/2}(\partial\Omega), H^{-1/2}(\partial\Omega))$. As an application of the stability, we consider in section 5 mollified versions γ_λ of a piecewise continuous conductivity distribution γ and show that reconstructions of γ_λ converge to reconstructions of γ as $\lambda \to 0$. This means that no systematic artifacts are introduced when the reconstruction method is applied to conductivities outside the assumptions of the theory.

In section 6, a connection between the linearization method of Calderón [7] and the D-bar method is established. Calderón's method is written in terms of $\mathbf{t}^{\exp}$ and is revealed to be a low-order approximation to the D-bar method. The simple example of the unit disk containing one concentric ring of constant conductivity with a discontinuity at the interface is studied in depth in section 7. We write $\mathbf{t}^{\exp}$ as a series showing the asymptotic growth rate. Reconstructions by Calderón's method and the D-bar method with the $\mathbf{t}^{\exp}$ approximation are expressed in explicit formulas.

In section 8, we illustrate our theoretical findings by numerical examples. We find that both the D-bar method and Calderón's method can approximately recover the location of a discontinuity. Also, both methods yield good reconstructions of low-contrast conductivities but have difficulties in recovering the actual conductivity values in the presence of high contrast features near the boundary.

2. The D-bar reconstruction method. In this section, we briefly review the reconstruction method based on the proof by Nachman [25]. We will describe both the exact mathematical algorithm and an approximate numerical algorithm.

2.1. Exact reconstruction from infinite precision data. The reconstruction method uses exponentially growing solutions to the conductivity equation. Suppose $\gamma - 1 \in W^{1+\epsilon,p}(\mathbb{R}^2)$ with $p > 2$ and $\gamma \equiv 1$ in $\mathbb{R}^2 \setminus \overline{\Omega}$. Then the equation

$$\nabla \cdot \gamma \nabla u = 0 \text{ in } \mathbb{R}^2 \tag{5}$$

has a unique exponentially growing solution u that behaves like e^{ixk}, where x is understood as $x = x_1 + ix_2 \in \mathbb{C}$ and the parameter $k = k_1 + ik_2 \in \mathbb{C}$. The construction of exponentially growing solutions is done by reducing the conductivity equation to either a Schrödinger equation (requires two derivatives on the conductivity) or a first-order system (requires one derivative). Consider $\psi := u\sqrt{\gamma}$ satisfying $(e^{-ixk}\psi(x,k) - 1) \in W^{1,p}(\mathbb{R}^2)$ with $p > 2$, and note that since $\gamma = 1$ at $\partial\Omega$ we have $u|_{\partial\Omega} = \psi|_{\partial\Omega}$. The intermediate object in the reconstruction method is the scattering transform defined in terms of the DN map by (3).

The reconstruction algorithm consists of the two steps

$$\Lambda_\gamma \to \mathbf{t} \to \gamma. \tag{6}$$

In order to compute $\mathbf{t}$ from Λ_γ by (3), one needs to find the trace of $\psi(\cdot,k)$ on $\partial\Omega$. It turns out that $\psi|_{\partial\Omega}$ satisfies

$$\psi(\cdot,k)|_{\partial\Omega} = e^{ikx} - S_k(\Lambda_\gamma - \Lambda_1)\psi(\cdot,k). \tag{7}$$

Here S_k is the single-layer operator

$$(S_k\phi)(x) := \int_{\partial\Omega} G_k(x-y)\phi(y)d\sigma(y), \quad k \in \mathbb{C}\setminus 0, \tag{8}$$

where the Faddeev's Green's function G_k is defined by

$$G_k(x) := \frac{e^{ikx}}{(2\pi)^2}\int_{\mathbb{R}^2} \frac{e^{ix\cdot\xi}}{|\xi|^2 + 2k(\xi_1 + i\xi_2)}d\xi, \quad -\Delta G_k = \delta. \tag{9}$$

Here the dot product is computed with real vectors $x = (x_1, x_2)$ and $\xi = (\xi_1, \xi_2)$. The Fredholm equation (7) is uniquely solvable in $H^{1/2}(\partial\Omega)$; see [25].

To compute γ from $\mathbf{t}$, the key observation is that with respect to the parameter k, the function $\mu(x,k) = e^{-ixk}\psi(x,k)$ satisfies a differential equation where $\mathbf{t}$ enters as a coefficient. More precisely, μ satisfies for fixed $x \in \mathbb{C}$ the D-bar equation

$$\overline{\partial}_k\mu(x,k) = \frac{1}{4\pi\overline{k}}\mathbf{t}(k)e_{-x}(k)\overline{\mu(x,k)}, \quad k \in \mathbb{C}, \tag{10}$$

where the unimodular function e_k is defined by

$$e_x(k) := e^{i(kx+\overline{k}\bar{x})} = e^{-i(-2k_1,2k_2)\cdot x}. \tag{11}$$

It is shown in [25] (see also [6, 20]) that $\mu(x,\cdot)$ is, in fact, the unique solution to (10) defined by the asymptotic condition $\mu(x,\cdot) - 1 \in L^r(\mathbb{R}^2), r > 2/\epsilon$. Moreover, the solution belongs to $C^\alpha(\mathbb{R}^2)$ with $\alpha < 1$; see section 3. Hence $\mu(x,k)$ can be computed from $\mathbf{t}$ by solving (10) or, equivalently, the Fredholm integral equation

$$\mu(x,s) = 1 + \frac{1}{(2\pi)^2}\int_{\mathbb{R}^2} \frac{\mathbf{t}(k)}{(s-k)\overline{k}}e_{-x}(k)\overline{\mu(x,k)}dk_1dk_2. \tag{12}$$

Finally, the conductivity can be recovered from μ using the formula

$$\gamma(x) = \mu(x,0)^2, \quad x \in \Omega. \tag{13}$$

2.2. Truncation of scattering transform. Note that in (12) the integral is over the whole plane. We will define a regularized D-bar algorithm by truncating the scattering transform to a disk of radius R. Then

$$\mathbf{t}_{\mathrm{R}}(k) \equiv \begin{cases} \mathbf{t}(k) & \text{for } |k| \le R, \\ 0 & \text{for } |k| > R, \end{cases} \tag{14}$$

and $\mu_{\mathrm{R}}(x,k)$ is the solution of

$$\mu_{\mathrm{R}}(x,s) = 1 + \frac{1}{(2\pi)^2}\int_{|k|\le R} \frac{\mathbf{t}_{\mathrm{R}}(k)}{(s-k)\overline{k}}e_{-x}(k)\overline{\mu_{\mathrm{R}}(x,k)}dk_1dk_2. \tag{15}$$

This defines a modified D-bar algorithm consisting of the following steps:

1. Solve (7) for $\psi|_{\partial\Omega}$.
2. Compute $\mathbf{t}_{\mathrm{R}}$ by (3) and (14).
3. Solve the integral equation (15) for μ_{R}.
4. Compute the reconstruction $\gamma_{\mathrm{R}}(x) = \mu_{\mathrm{R}}(x,0)^2$.

According to [24], this algorithm gives correct results at the asymptotic limit $R \to \infty$.

2.3. Approximate reconstruction from finite precision data. In the presence of noise in the data, solving (7) is difficult, and therefore the approximate scattering transform $\mathbf{t}^{\exp}(k)$ defined by (4) was introduced. An advantage of $\mathbf{t}^{\exp}(k)$ is that the definition applies just as well to discontinuous conductivities as to smooth ones. However, it can be shown in certain cases that $\mathbf{t}^{\exp}(k)$ grows so fast as $|k|$ tends to infinity (see (64) below) that the corresponding D-bar equation is not solvable. In addition, the practical computation is stable only for $|k| \le R$, where the radius R depends on the noise level. Thus the scattering transform needs to be truncated. Set

$$\mathbf{t}_{\mathrm{R}}^{\exp}(k) = \begin{cases} \mathbf{t}^{\exp}(k) & \text{for } |k| \le R, \\ 0 & \text{for } |k| > R, \end{cases} \tag{16}$$

and write the corresponding D-bar equation:

$$\mu_{\mathrm{R}}^{\exp}(x,s) = 1 + \frac{1}{(2\pi)^2} \int_{|k|\le R} \frac{\mathbf{t}_{\mathrm{R}}^{\exp}(k)}{(s-k)\overline{k}} e_{-x}(k) \overline{\mu_{\mathrm{R}}^{\exp}(x,k)} dk_1 dk_2. \tag{17}$$

We arrive at the following reconstruction algorithm:

1. Compute $\mathbf{t}_{\mathrm{R}}^{\exp}$ by (4) and (16).
2. Solve (17) for $\mu_{\mathrm{R}}^{\exp}$.
3. Compute $\gamma_{\mathrm{R}}^{\exp}(x) = \mu_{\mathrm{R}}^{\exp}(x,0)^2$.

We will show in section 4 that this reconstruction algorithm is robust against noise. In the numerical implementation, the challenge is to solve (17); see [29, 21].

3. Smoothness of reconstructions from truncated scattering data. We first investigate the x-smoothness of the solution to the D-bar equation

$$\mu(x,s) = 1 + \frac{1}{\pi} \int_{\mathbb{R}^2} \frac{\phi(k)}{s-k} e_{-x}(k) \overline{\mu(x,k)} dk_1 dk_2 \tag{18}$$

under various assumptions on the coefficient ϕ. Then we will show that the reconstructions γ_{R} and $\gamma_{\mathrm{R}}^{\exp}$ computed from truncated scattering data are smooth functions.

The analysis of (18) makes heavy use of the solid Cauchy transform

$$\mathcal{C}f(s) := \frac{1}{\pi} \int_{\mathbb{R}^2} \frac{f(k)}{s-k} dk_1 dk_2. \tag{19}$$

The following result is essentially [25, Lemma 1.2] and [35, Theorem 1.21].

LEMMA 3.1. *Suppose $f \in L^{p_1}(\mathbb{R}^2)$, where $1 < p_1 < 2$. Then*

$$\|\mathcal{C}f\|_{L^{\tilde{p}_1}(\mathbb{R}^2)} \le C \|f\|_{L^{p_1}(\mathbb{R}^2)}, \quad \frac{1}{\tilde{p}_1} = \frac{1}{p_1} - \frac{1}{2}. \tag{20}$$

Suppose further that $f \in L^{p_1}(\mathbb{R}^2) \cap L^{p_2}(\mathbb{R}^2)$, where $1 < p_1 < 2 < p_2 < \infty$. Then

$$\|\mathcal{C}f\|_{C^\alpha(\mathbb{R}^2)} \le C(\|f\|_{L^{p_1}(\mathbb{R}^2)} + \|f\|_{L^{p_2}(\mathbb{R}^2)}), \quad \alpha = 1 - \frac{2}{p_2}. \tag{21}$$

In the next lemma, we consider the continuity of the Cauchy transform applied to functions depending on a parameter. To simplify notation, we introduce for $x \in \mathbb{R}^2$ the real-linear operator Φ_x by $\Phi_x f = \phi(k) e_{-k}(x) \overline{f(k)}$.

LEMMA 3.2. *Let $\phi \in L^{p_1} \cap L^{p_2}(\mathbb{R}^2)$ with $1 < p_1 < 2 < p_2 < \infty$. Then the map*

$$x \mapsto \mathcal{C}(\phi e_{-x}) \tag{22}$$

is continuous from $\mathbb{R}^2$ *into* $L^{\widetilde{p}_1}(\mathbb{R}^2) \cap C^\alpha(\mathbb{R}^2)$, $\alpha = 1 - 2/p_2$. *Further,* $\mathcal{C}\Phi_x$ *is bounded on* $L^r(\mathbb{R}^2)$, $r > 2$, *and the map* $x \mapsto \mathcal{C}\Phi_x$ *is continuous from* $\mathbb{R}^2$ *into* $\mathcal{L}(L^r(\mathbb{R}^2))$.

Proof. Using the Lebesgue dominated convergence theorem, it is straightforward to see that the map $x \mapsto \phi e_{-x}$ is continuous from $\mathbb{R}^2$ into $L^{p_1}(\mathbb{R}^2) \cap L^{p_2}(\mathbb{R}^2)$. The continuity of the map (22) then follows from the linearity of $\mathcal{C}$ and (20)–(21).

The assumption on ϕ implies by the Hölder inequality that $\phi(k)e_{-k}(x) \in L^2(\mathbb{R}^2)$, and, as before, we can argue that $\phi(k)e_{-k}(x)$ is continuous with respect to $x \in \mathbb{R}^2$. It follows then by the Hölder inequality that $\Phi_x \in \mathcal{L}(L^r(\mathbb{R}^2), L^{2r/(2+r)}(\mathbb{R}^2))$. Moreover, Φ_x is continuous with respect to $x \in \mathbb{R}^2$. The claim for $\mathcal{C}\Phi_x$ then follows from (20). ∎

We are now ready to prove the unique solvability of (18) in the case where ϕ is in certain L^p-spaces and analyze how the solution depends on the parameter x.

LEMMA 3.3. *Let* $\phi \in L^{p_1} \cap L^{p_2}(\mathbb{R}^2)$ *with* $1 < p_1 < 2 < p_2 < \infty$. *Then* (18) *has a unique solution* μ *with* $\mu(x,\cdot) - 1 \in L^r \cap C^\alpha(\mathbb{R}^2)$ *for any* $r \geq \widetilde{p}_1$ *and* $\alpha < 1 - 2/p_2$. *Moreover, the map*

$$x \mapsto \mu(x,\cdot) \tag{23}$$

is continuous from $\mathbb{R}^2$ *into* $L^r \cap C^\alpha(\mathbb{R}^2)$.

Proof. Equation (18) is equivalent to the integral equation

$$(I - \mathcal{C}\Phi_x)(\mu - 1) = \mathcal{C}\Phi_x(1). \tag{24}$$

Note that $\mathcal{C}\Phi_x(1) \in L^r(\mathbb{R}^2)$ for any $r \geq \widetilde{p}_1$. Now, from Lemma 3.2, we know that $\mathcal{C}\Phi_x$ is bounded on $L^r(\mathbb{R}^2)$, $r > 2$. Moreover, the operator is compact (see [26, Lemma 4.2]), and hence (24) is a Fredholm equation of the second kind. Since the associated homogeneous equation has only the trivial solution (see, for instance, [6]), we can define

$$\mu - 1 = [I - \mathcal{C}\Phi_x]^{-1}(\mathcal{C}\Phi_x(1)) \in L^r(\mathbb{R}^2), \quad r \geq \widetilde{p}_1. \tag{25}$$

By (21),

$$\mathcal{C}\Phi_x(1) \in C^\alpha(\mathbb{R}^2), \quad \alpha = 1 - \frac{2}{p_2}, \tag{26}$$

$$\mathcal{C}\Phi_x(\mu - 1) \in C^\alpha(\mathbb{R}^2), \quad \alpha < 1 - \frac{2}{p_2}, \tag{27}$$

and then the Hölder regularity of $\mu - 1$ is obtained from (24).

Next, we show continuity of the map $x \mapsto (\mu(x,\cdot) - 1)$ from $\mathbb{R}^2$ into $L^r(\mathbb{R}) \cap C^\alpha(\mathbb{R}^2)$. By Lemma 3.2, we know that $\mathcal{C}\Phi_x 1 \in L^r(\mathbb{R}^2) \cap C^\alpha(\mathbb{R}^2)$ depends continuously on x.

Also, by Lemma 3.2, the map $x \mapsto \mathcal{C}\Phi_x$ is continuous from $\mathbb{R}^2$ to $\mathcal{L}(L^r(\mathbb{R}^2))$. Since the operator $I - \mathcal{C}\Phi_x$ is invertible for all $x \in \mathbb{R}^2$, the map $x \mapsto [I - \mathcal{C}\Phi_x]^{-1}$ is continuous from $\mathbb{R}^2$ to $\mathcal{L}(L^r(\mathbb{R}^2))$ as well. Hence the right-hand side of (25) depends continuously on x as a map from $\mathbb{R}^2$ into $L^r(\mathbb{R}^2)$. The continuity into $C^\alpha(\mathbb{R}^2)$ now follows as before from (21) and (24). ∎

Next, we consider the solvability of (18) in the case where ϕ is compactly supported.

LEMMA 3.4. *Suppose* $\phi \in L^p(\mathbb{R}^2)$, $p > 2$, *is compactly supported. Then* (18) *has a unique solution* μ *with* $\mu - 1 \in L^r \cap C^\alpha(\mathbb{R}^2), r > 2, \alpha < 1 - 2/p$. *Moreover, the map*

$$x \mapsto \mu(x,\cdot) - 1 \tag{28}$$

is smooth from $\mathbb{R}^2$ *into* $L^r \cap C^\alpha(\mathbb{R}^2)$.

Proof. Since $\phi \in L^{p_1} \cap L^p(\mathbb{R}^2)$ for $1 < p_1 < 2$, by Lemma 3.3, (18) has a unique solution μ with $\mu - 1 \in L^r \cap C^\alpha(\mathbb{R}^2), r > 2, \alpha < 1 - 2/p$, depending continuously on x.

To prove that μ is smooth, we will show first that $\partial_{x_1}\mu$ is continuous. By applying the differential operator ∂_{x_1} to (18), it follows that ∂_{x_1} satisfies the equation

$$\overline{\partial}_k \partial_{x_1}\mu = \phi(k)e_{-k}\overline{\partial_{x_1}\mu} - \phi(k)k_1 e_{-k}\overline{\mu}. \tag{29}$$

Since $\mu - 1 \in L^r(\mathbb{R}^2)$ for any $r > 2$, we have $\phi(k)k_1 e_{-k}\overline{\mu} \in L^q(\mathbb{R}^2)$ for any $q < p$. Hence $\mathcal{C}(\phi(k)k_1 e_{-k}\overline{\mu}) \in L^r(\mathbb{R}^2)$ for any $r > 2$. Equation (29) then has the unique solution

$$\partial_{x_1}\mu = -(I - \mathcal{C}\Phi_x)^{-1}(\phi(k)k_1 e_{-k}\overline{\mu}) \in L^r(\mathbb{R}^2) \cap C^\alpha(\mathbb{R}^2), \quad r > 2, \quad \alpha < 1 - 2/p.$$

Since $(\phi(k)k_1 e_{-k}\overline{\mu})$ and $(I - \mathcal{C}\Phi_x)^{-1}$ are continuous with respect to x, so is $\partial_{x_1}\mu$. Using induction, this argument can easily be extended to show that all x-derivatives of μ are continuous, i.e., that μ is smooth. ∎

We can now show using Lemma 3.3 that (12) admits a unique solution. Moreover, by using Lemma 3.4, we can show that (15) and (17) are uniquely solvable and that the solutions are smooth functions of the x-variable.

PROPOSITION 3.5. *Let* $\Omega \subset \mathbb{R}^2$ *be the unit disc, and suppose* γ *satisfies* (1) *with* $\gamma = 1$ *near* $\partial\Omega$.

(a) *Suppose further that* $\gamma \in W^{1+\epsilon,p}(\Omega)$ *with* $2 < p$. *Then for each* $x \in \mathbb{R}^2$ *and* $R > 0$, (12) *and* (15) *have unique solutions* μ, μ_R, *respectively, which satisfy* $\mu(x, \cdot) - 1 \in L^r \cap \mathbb{C}^\alpha(\mathbb{R}^2), r > 2/\epsilon, \alpha < 1$, *and* $(\mu_R(x, \cdot) - 1) \in L^r \cap C^\alpha(\mathbb{R}^2), r > 2, \alpha < 1$. *Furthermore,* $\mu_R(x, \cdot)$ *is smooth with respect to* x.

(b) *For* $x \in \mathbb{R}^2$ *and* $R > 0$, (17) *has a unique solution* $\mu_R^{\exp}(x, \cdot)$ *with* $\mu_R^{\exp}(x, \cdot) - 1 \in L^r \cap C^\alpha(\mathbb{R}^2), r > 2, \alpha < 1$, *which is smooth with respect to* x.

Proof. To prove (a), we use the fact from [18, 20] that $\mathbf{t}(k)/\overline{k} \in L^p(\mathbb{R}^2), 2 - \epsilon < p < \infty$. Hence $\phi(k) = \mathbf{t}(k)/(4\pi\overline{k})$ satisfies the assumptions in Lemma 3.3, and the claim follows. Furthermore, $\phi = \mathbf{t}_{\mathrm{R}}/(4\pi\overline{k})$ satisfies the assumptions in Lemma 3.4. It follows that (15) has a unique solution μ_{R} with the indicated properties.

To prove (b), we note that $\mathbf{t}_{\mathrm{R}}^{\exp}$ is a bounded function with compact support. Then again we use Lemma 3.4. ∎

As a consequence of this proposition, it follows that the reconstructions $\gamma_{\mathrm{R}}(x) = (\mu_{\mathrm{R}}(x, 0))^2$ and $\gamma_{\mathrm{R}}^{\exp} = (\mu_{\mathrm{R}}^{\exp}(x, 0))^2$ based on truncated scattering data are smooth functions.

4. Stability of the approximate reconstruction method. In this section, we show that the reconstruction method using the truncated $\mathbf{t}^{\exp}$ is stable. We will start by formulating the reconstruction procedure as an operator. Let $L_c^p(\mathbb{R}^2)$ denote the space of $L^p(\mathbb{R}^2)$ functions with compact support, and define for $k \in \mathbb{C}$ the linear operator $\mathcal{T}_{\mathrm{R}}^{\exp} : \mathcal{L}(H^{1/2}(\partial\Omega), H^{-1/2}(\partial\Omega)) \to L_c^\infty(\mathbb{R}^2)$ by

$$(\mathcal{T}_{\mathrm{R}}^{\exp} L)(k) = \chi_{|k|<R} \frac{1}{4\pi\overline{k}} \int_{\partial\Omega} (e^{i\overline{kx}} - 1)L(e^{ikx} - 1)d\sigma(x). \tag{30}$$

Define further for $p > 2$ the nonlinear operator

$$\mathcal{S} : L_c^p(\mathbb{R}^2) \to C^\infty(\overline{\Omega}), \quad \phi \mapsto \mu(x, 0),$$

where $\mu(x,\cdot)$ is the unique solution to (10) (see Lemma 3.4). By composition, we then define $\mathcal{M}_{\mathrm{R}}^{\exp} : \mathcal{L}(H^{1/2}(\partial\Omega), H^{-1/2}(\partial\Omega)) \to C^\infty(\overline{\Omega})$ by

$$\mathcal{M}_{\mathrm{R}}^{\exp} = \mathcal{S} \circ \mathcal{T}_{\mathrm{R}}^{\exp}. \tag{31}$$

Using this notation, it is clear that

$$(\gamma_{\mathrm{R}}^{\exp}(x))^{1/2} = \mu_{\mathrm{R}}^{\exp}(x,0) = \mathcal{M}_{\mathrm{R}}^{\exp}(\Lambda_\gamma - \Lambda_1), \tag{32}$$

since $(\Lambda_\gamma - \Lambda_1)1 = 0$ and $\int_{\partial\Omega}(\Lambda_\gamma - \Lambda_1) f d\sigma(x) = 0$ for all $f \in H^{1/2}(\partial\Omega)$. Thus $\mathcal{M}_{\mathrm{R}}^{\exp}$ is an operator that implements the reconstruction algorithm based on the truncated approximate scattering data.

The main goal of this section is to show that $\mathcal{M}_{\mathrm{R}}^{\exp}$ is continuous as an operator from $\mathcal{L}(H^{1/2}(\partial\Omega), H^{-1/2}(\partial\Omega))$ into $C^\infty(\overline{\Omega})$. This will show that the reconstruction algorithm using $\mathbf{t}_{\mathrm{R}}^{\exp}$ is stable.

LEMMA 4.1. *The operator $\mathcal{T}_R^{\exp}$ is bounded from $\mathcal{L}(H^{1/2}(\partial\Omega), H^{-1/2}(\partial\Omega))$ into $L_c^\infty(\mathbb{R}^2)$ and satisfies*

$$\|\mathcal{T}_{\mathrm{R}}^{\exp} L\|_{L^\infty(\mathbb{R}^2)} \le C e^{2R} \|L\|_{\mathcal{L}(H^{1/2}(\partial\Omega), H^{-1/2}(\partial\Omega))}. \tag{33}$$

Proof. For $|k| < R$, it is straightforward to obtain the estimate

$$|\mathcal{T}_{\mathrm{R}}^{\exp} L(k)| \le C \frac{1}{|k|} \|e^{ikx} - 1\|^2_{H^{1/2}(\partial\Omega)} \|L\|_{\mathcal{L}(H^{1/2}(\partial\Omega), H^{-1/2}(\partial\Omega))}.$$

Hence (33) follows from the uniform estimate $\|e^{ikx} - 1\|_{H^{1/2}(\partial\Omega)} \le C|k|^{1/2} e^{|k|}$. ∎

Next, we consider the solution operator $\mathcal{S}$. A stability estimate for this operator was given in [18, Lemma 3.1.5]; we will generalize this result slightly. The aim is to show that the solution μ to (18) depends continuously on the coefficient ϕ. Let $\mu_j, j = 1, 2$, be the solution to

$$\begin{aligned} \mu_j(x,s) - 1 = {} & \frac{1}{\pi} \int_{\mathbb{R}^2} \frac{\phi_j(k)}{s-k} e_{-x}(k) (\overline{\mu_j(x,k)} - 1) dk_1 dk_2 \\ & + \frac{1}{\pi} \int_{\mathbb{R}^2} \frac{\phi_j(k)}{s-k} e_{-x}(k) dk_1 dk_2, \quad j = 1, 2. \end{aligned} \tag{34}$$

Then we have the following result.

LEMMA 4.2. *Let $1 < p_1 < 2 < p_2 < \infty$ with $0 < 1/p_1 + 1/p_2 - 1/2 < 1/2$, and suppose $\phi_j \in L^{p_1}(\mathbb{R}^2) \cap L^{p_2}(\mathbb{R}^2)$, $j = 1, 2$. Further, let $x \in \overline{\Omega}$. Then, for the solution $\mu_j(x,\cdot)$ to (34), we have the estimate*

$$\|\mu_1(x,\cdot) - \mu_2(x,\cdot)\|_{C^\alpha(\mathbb{R}^2)} \le C K_1 K_2 \|\phi_1 - \phi_2\|_{L^{p_1}(\mathbb{R}^2) \cap L^{p_2}(\mathbb{R}^2) \cap L^2(\mathbb{R}^2) \cap L^q(\mathbb{R}^2)}, \tag{35}$$

where $\alpha < 1 - 2/q$, $1/q = 1/p_2 + 1/p_1 - 1/2$, and $K_j = \exp(C\|\phi_j\|_{L^{p_1}(\mathbb{R}^2) \cap L^{p_2}(\mathbb{R}^2)})$. If $\phi_1, \phi_2 \in L_c^p(\mathbb{R}^2)$, $p > 2$, we have the estimate

$$\|\mu_1(x,\cdot) - \mu_2(x,\cdot)\|_{C^\alpha(\mathbb{R}^2)} \le C K_1 K_2 \|\phi_1 - \phi_2\|_{L^p(\mathbb{R}^2)} \tag{36}$$

for $\alpha < 1 - 2/p$.

Proof. From [4, Lemma 2.6], we know that if $a \in L^{p_1}(\mathbb{R}^2) \cap L^{p_2}(\mathbb{R}^2)$ for $1 < p_1 < 2 < p_2 < \infty$ and $b \in L^p(^2)$ for $1 < p < 2$, then the solution to the integral equation

$$m = \mathcal{C}(a\overline{m}) + \mathcal{C}(b)$$

satisfies the estimate

$$\|m\|_{L^{\tilde{p}}(\mathbb{R}^2)} \le C\exp(C\|a\|_{L^{p_1}(\mathbb{R}^2)\cap L^{p_2}(\mathbb{R}^2)})\|b\|_{L^p(\mathbb{R}^2)}. \tag{37}$$

Applied to (34), the estimate reads

$$\|\mu_1(x,\cdot)-1\|_{L^{\widetilde{p_1}}(\mathbb{R}^2)} \le CK_1\|\phi_1\|_{L^{p_1}(\mathbb{R}^2)}. \tag{38}$$

Since

$$\begin{aligned}\mu_1(x,s)-\mu_2(x,s) &= \frac{1}{\pi}\int_{\mathbb{R}^2}\frac{\phi_2(k)}{s-k}e_{-x}(k)(\overline{\mu_1-\mu_2})dk_1dk_2\\ &\quad+\frac{1}{\pi}\int_{\mathbb{R}^2}\frac{\phi_1(k)-\phi_2(k)}{s-k}e_{-x}(k)\overline{\mu_1(x,k)}dk_1dk_2,\end{aligned} \tag{39}$$

the estimate (37) applied to $\mu_1-\mu_2$ then gives

$$\begin{aligned}\|\mu_1-\mu_2\|_{L^{\widetilde{p_1}}(\mathbb{R}^2)} &\le CK_2\|(\phi_1-\phi_2)\mu_1\|_{L^{p_1}(\mathbb{R}^2)}\\ &\le CK_2\big(\|\phi_1-\phi_2\|_{L^{p_1}(\mathbb{R}^2)}+\|\phi_1-\phi_2\|_{L^2(\mathbb{R}^2)}\|\mu_1-1\|_{L^{\widetilde{p_1}}(\mathbb{R}^2)}\big)\\ &\le CK_2\left(\|\phi_1-\phi_2\|_{L^{p_1}(\mathbb{R}^2)}+\|\phi_1-\phi_2\|_{L^2(\mathbb{R}^2)}\Phi_1\|\phi_1\|_{L^{p_1}(\mathbb{R}^2)}\right),\end{aligned} \tag{40}$$

where we have used (38). To get the Hölder estimate, we use (39) and (21) to obtain

$$\|\mu_1-\mu_2\|_{C^\alpha(\mathbb{R}^2)} \le \|\phi_2(\mu_1-\mu_2)\|_{L^q(\mathbb{R}^2)}+\|(\phi_1-\phi_2)\mu_1\|_{L^q(\mathbb{R}^2)} \tag{41}$$

for $q>2$ and $\alpha=1-2/q$. By choosing $1/q=1/p_2+1/\widetilde{p_1}$ ($<1/2$ by assumption), we have by (40) and (38)

$$\begin{aligned}\|\phi_2(\mu_1-\mu_2)\|_{L^q(\mathbb{R}^2)} &\le \|\phi_2\|_{L^{p_2}(\mathbb{R}^2)}\|\mu_1-\mu_2\|_{L^{\widetilde{p_1}}(\mathbb{R}^2)}\\ &\le \|\phi_2\|_{L^{p_2}(\mathbb{R}^2)}CK_2\big(\|\phi_1-\phi_2\|_{L^{p_1}(\mathbb{R}^2)}\\ &\quad+\|\phi_1-\phi_2\|_{L^2(\mathbb{R}^2)}K_1\|\phi_1\|_{L^{p_1}(\mathbb{R}^2)}\big)\end{aligned} \tag{42}$$

$$\begin{aligned}\|(\phi_1-\phi_2)\mu_1\|_{L^q(\mathbb{R}^2)} &\le \|\phi_1-\phi_2\|_{L^{p_2}(\mathbb{R}^2)}\|\mu_1-1\|_{L^{\widetilde{p_1}}(\mathbb{R}^2)}+\|\phi_1-\phi_2\|_{L^q(\mathbb{R}^2)}\\ &\le \|\phi_1-\phi_2\|_{L^{p_2}(\mathbb{R}^2)}CK_1\|\phi_1\|_{L^{p_1}(\mathbb{R}^2)}+\|\phi_1-\phi_2\|_{L^q(\mathbb{R}^2)}.\end{aligned} \tag{43}$$

Combining (41) with (42) and (43) gives (35).

Finally, (36) follows from (35) by using the compact support of ϕ_1,ϕ_2. ∎

As a direct consequence of the lemma, we obtain the following result.

COROLLARY 4.3. *The operator $\mathcal{S}$ is bounded from $L^p_c(\mathbb{R}^2)$, $p>2$, into $L^\infty(\Omega)$ and*

$$\|\mathcal{S}(\phi_1)-\mathcal{S}(\phi_2)\|_{L^\infty(\Omega)} \le C\|\phi_1-\phi_2\|_{L^p(\mathbb{R}^2)}, \tag{44}$$

where C depends on p, the support of ϕ_1,ϕ_2, and $\|\phi_1\|_{L^p(\mathbb{R}^2)},\|\phi_2\|_{L^p(\mathbb{R}^2)}$.

Proof. For fixed $x\in\overline{\Omega}$, (36) implies that

$$|\mathcal{S}(\phi_1)-\mathcal{S}(\phi_2)| = |\mu_1(x,0)-\mu_2(x,0)| \le C\Phi_1\Phi_2\|\phi_1-\phi_2\|_{L^p(\mathbb{R}^2)}.$$

This proves the result. ∎

We have now seen that the linear operator $\mathcal{T}_{\mathrm{R}}^{\exp}$ is bounded and the operator $\mathcal{S}$ is continuous. This enables us to conclude that $\mathcal{M}_{\mathrm{R}}^{\exp}=\mathcal{S}\circ\mathcal{T}_{\mathrm{R}}^{\exp}$ is continuous.

5. Convergence of reconstructions of mollified conductivities. Conductivities in practical applications of EIT are often piecewise smooth, but the theory of D-bar method covers only differentiable conductivities. We exclude the possibility of systematic artifacts introduced by discontinuities by proving the following: smooth approximations to nonsmooth conductivities yield almost the same reconstructions.

Let $\Omega = B(0,1)$. Let $c_0 > 0$ and $0 < R < 1$, and define $X = X(c_0, R) \subset L^\infty(\Omega)$ by

$$X = \{\gamma \in L^\infty(\Omega) \mid c_0^{-1} \le \gamma \le c_0,\ \mathrm{supp}(\gamma - 1) \subset B(0,R)\}.$$

The following lemma contains a continuity result for the operator $\gamma \mapsto \Lambda_\gamma$.

LEMMA 5.1. *Let $\gamma, \gamma_j \in X, j \in \mathbb{N}$, and suppose $\gamma_j \to \gamma$ a.e. Then, for any $s \in \mathbb{R}$, $\Lambda_{\gamma_j} - \Lambda_\gamma \longrightarrow 0$ in the strong topology of $\mathcal{L}(H^{1/2}(\partial\Omega), H^s(\partial\Omega))$.*

Proof. Let $f \in H^{1/2}(\partial\Omega)$. Let $\gamma_0 = \gamma$, and define $u_j, j = 0, 1, 2, \ldots$, as the unique solution to $\nabla \cdot \gamma_j \nabla u_j = 0$ in Ω, $u_j|_{\partial\Omega} = f$. Then

$$\|u_0\|_{H^1(\Omega)} \le C_2 \|f\|_{H^{1/2}}, \tag{45}$$

where the constant C_2 depends only on the uniform ellipticity constant c_0. Since

$$\nabla \cdot \gamma_j \nabla (u_j - u_0) = \nabla \cdot (\gamma - \gamma_j) \nabla u_0, \quad (u_j - u_0)|_{\partial\Omega} = 0,$$

there is a constant C_3 (depending only on c_0) such that the estimate

$$\|(u_j - u_0)\|_{H^1(\Omega)} \le C_3 \|(\gamma - \gamma_j)\nabla u_0\|_{L^2(\Omega)} \tag{46}$$

holds. Furthermore, $\Delta(u_j - u_0) = 0$ and $\partial_\nu (u_j - u_0)|_{\partial\Omega} = 0$ in the region $\Omega \setminus B(0,R)$. Therefore we can extend (46) to

$$\|(u_j - u_0)\|_{H^s(\Omega \setminus B(0,R_1))} \le C_4 \|(\gamma - \gamma_j)\nabla u_0\|_{L^2(\Omega)},$$

for any $s \in \mathbb{R}$, where C_4 depends on s, c_0, and $R_1 \in (R, 1)$. By taking normal derivative at the boundary, we then obtain, for any $s \in \mathbb{R}$,

$$\|(\Lambda_{\gamma_j} - \Lambda_\gamma) f\|_{H^s(\partial\Omega)} \le C_5 \|(\gamma - \gamma_j)\nabla u_0\|_{L^2(\Omega)}, \tag{47}$$

where C_5 depends on s, c_0, and R.

To consider convergence in the strong topology, let us fix f and γ, implying that u_0 can be considered as a fixed function. Then using Lebesgue dominated convergence, it follows that $\lim_{j\to\infty} \|(\gamma - \gamma_j)\nabla u_0\|_{L^2(\Omega)} = 0$. By (47), this implies the claim. ∎

The next lemma shows that a strongly convergent sequence of operators is norm convergent when composed with a compact operator defined on a Hilbert space.

LEMMA 5.2. *Let X, Y be Banach spaces and H be a separable Hilbert space. Suppose $T, T_j \in \mathcal{L}(X,Y)$, $j = 1, 2, \ldots$, and $K \in \mathcal{L}(H,X)$ is compact. If $T_j \to T$ as $j \to \infty$ in the strong topology of $\mathcal{L}(X,Y)$, then $T_j K \to TK$ as $j \to \infty$ in the norm topology of $\mathcal{L}(H,Y)$.*

Proof. By the principle of uniform boundedness, there is a constant C_0 such that $\|T\|_{\mathcal{L}(X,Y)} < C_0$ and $\|T_j\|_{\mathcal{L}(X,Y)} < C_0$ for all j.

Since the compact operator K maps from a separable Hilbert space into a Banach space, there is a sequence of finite rank operators $K_n, n \in \mathbb{N}$, with $\mathrm{rank}(K_n) = n$ that converges in norm to K (see [28, Theorem 6.13] for a proof of this fact in the Hilbert space case; the proof is the same in our case). Fix $\epsilon > 0$, and take n such that

$$\|K - K_n\|_{\mathcal{L}(H,X)} < \epsilon.$$

Further, since K_n has finite rank, there is a $J = J(\epsilon) \geq 0$ such that, for $j \geq J$,

$$\|(T_j - T)K_n\|_{\mathcal{L}(H,Y)} \leq \epsilon.$$

Hence, for $j \geq J$,

$$\|(T_j - T)K\|_{\mathcal{L}(H,Y)} \leq \|T_j(K - K_n) + (T_j - T)K_n + T(K_n - K)\|_{\mathcal{L}(H,Y)} = 3C_0\epsilon.$$

This proves the result. ∎

We will now use the preceding lemma to prove norm convergence of the sequence of DN maps in Lemma 5.1.

LEMMA 5.3. *Let γ and γ_j be as in Lemma* 5.1. *Then*

$$\lim_{j\to\infty} \|\Lambda_{\gamma_j} - \Lambda_\gamma\|_{\mathcal{L}(H^{1/2}(\partial\Omega),H^{-1/2}(\partial\Omega))} = 0.$$

Proof. Since the inclusion operator $J\colon H^{1/2+r}(\partial\Omega) \to H^{1/2}(\partial\Omega)$ is compact for any $r > 0$, it follows from Lemmas 5.1 and 5.2 that

$$\lim_{j\to\infty} \|\Lambda_{\gamma_j} - \Lambda_\gamma\|_{\mathcal{L}(H^{\frac{1}{2}+r}(\partial\Omega),H^s(\partial\Omega))} = \lim_{j\to\infty} \|(\Lambda_{\gamma_j} - \Lambda_\gamma)J\|_{\mathcal{L}(H^{\frac{1}{2}+r}(\partial\Omega),H^s(\partial\Omega))} = 0 \tag{48}$$

for $r > 0, s \in \mathbb{R}$. Further, since $\gamma = \gamma_j = 1$ near $\partial\Omega$, $\Lambda_{\gamma_j} - \Lambda_\gamma$ is a smoothing pseudo-differential operator that can be extended to an operator $\mathcal{D}'(\partial\Omega) \to C^\infty(\partial\Omega)$. An application of Green's formula implies that the operator $\Lambda_{\gamma_j} - \Lambda_\gamma : \mathcal{D}'(\partial\Omega) \to C^\infty(\partial\Omega)$ and its transpose $(\Lambda_{\gamma_j} - \Lambda_\gamma)' : \mathcal{D}'(\partial\Omega) \to C^\infty(\partial\Omega)$ coincide. Thus (48) implies

$$\lim_{j\to\infty} \|\Lambda_{\gamma_j} - \Lambda_\gamma\|_{\mathcal{L}(H^{-s'}(\partial\Omega),H^{-1/2-r'}(\partial\Omega))} = 0 \tag{49}$$

for $r' > 0, s' \in \mathbb{R}$. Interpolation of (48) and (49) gives the result; see, for example, Theorem 5.1 and section 7.3 of [22] or formula (3.2) on p. 282 of [33]. ∎

Let $\gamma \in X(c_0, R)$ for some $c_0, R > 0$, and suppose that γ is continuous a.e. Let $\eta \in C_0^\infty(D(0, \alpha/2))$ be nonnegative and $\int_{\mathbb{R}^2} \eta = 1$. Define $\eta_\lambda(x) := \lambda^{-2}\eta(x/\lambda)$ for any $0 < \lambda < 1$, and set $\gamma_\lambda := \eta_\lambda * \gamma$. We then have the following result.

THEOREM 5.4. *Let $\gamma \in X(c_0, R)$ for some $c_0, R > 0$, and let γ_λ be defined as above. Let $\mathcal{M}_R^{\exp}$ be defined as in* (31). *Then we have*

$$\lim_{\lambda\to 0} \|\mathcal{M}_{\mathrm{R}}^{\exp}(\Lambda_{\gamma_\lambda} - \Lambda_\gamma)\|_{\mathcal{L}(L^\infty(\Omega),L^\infty(\Omega))} = 0.$$

Proof. As a consequence of the definition, there exist $\widetilde{c}_0, \widetilde{R} > 0$ such that $\gamma, \gamma_\lambda \in X(\widetilde{c}_0, \widetilde{R})$ for λ sufficiently small. Also $\gamma_\lambda \to \gamma$ a.e. Using Lemma 5.3, it follows that Λ_{γ_λ} converges to Λ_γ in the norm topology of $\mathcal{L}(H^{1/2}(\partial\Omega), H^{-1/2}(\partial\Omega))$. Finally, using the continuity of $\mathcal{M}_{\mathrm{R}}^{\exp}$ (see section 4), we conclude that the reconstruction $\mathcal{M}_{\mathrm{R}}^{\exp}(\Lambda_{\gamma_\lambda} - \Lambda_1)$ of $\gamma_\lambda^{1/2}$ converges to $\mathcal{M}_{\mathrm{R}}^{\exp}(\Lambda_\gamma - \Lambda_1)$. ∎

6. Connection to Calderón's linearization method. In the seminal paper [7], Calderón gave an algorithm for the reconstruction of conductivities close to constant (see also [38]). We write Calderón's method in the context of the approximate scattering transform $\mathbf{t}^{\exp}$ and compare it to the D-bar method.

6.1. Calderón's linearization method. Integrating by parts in (4) gives

$$\mathbf{t}^{\exp}(k) = \int_\Omega (\gamma - 1)\nabla u(x,k) \cdot \nabla(e^{i\overline{kx}})dx, \tag{50}$$

where

$$\nabla \cdot (\gamma - 1)\nabla u = 0 \text{ in } \Omega, \quad u|_{\partial\Omega} = e^{ikx}.$$

When $\|\gamma - 1\|_{L^\infty(\Omega)}$ is small, then u is close to e^{ikx} inside Ω. Indeed, if we write $u = e^{ikx} + \delta u$ for $\delta u \in H_0^1(\Omega)$ satisfying $\nabla \cdot \gamma \nabla \delta u = -\nabla \cdot (\gamma - 1)\nabla(e^{ikx})$, we have the estimate

$$\|\delta u\|_{H^1(\Omega)} \leq C\|\gamma - 1\|_{L^\infty(\Omega)} e^{|k|r}, \tag{51}$$

where r is the radius of the smallest ball containing Ω. Substituting $u = e^{ikx} + \delta u$ into (50) and dividing by $-2|k|^2$, we obtain

$$\begin{aligned} -\frac{\mathbf{t}^{\exp}(k)}{2|k|^2} &= -\frac{1}{2|k|^2}\int_\Omega (\gamma - 1)\nabla(e^{ikx} + \delta u) \cdot \nabla(e^{i\overline{kx}})dx \\ &= \int_\Omega (\gamma - 1)e_k(x)dx + R(k) \\ &= 2\pi \mathcal{F}(\chi_\Omega(\gamma - 1))(-2k_1, 2k_2) + R(k), \end{aligned} \tag{52}$$

where $\mathcal{F}$ denotes the Fourier transform and

$$R(k) = -\frac{1}{2|k|^2}\int_\Omega (\gamma - 1)\nabla \delta u \cdot \nabla(e^{i\overline{kx}})dx.$$

Using (51), it is not hard to obtain

$$|R(k)| \leq C\|\gamma - 1\|^2_{L^\infty(\Omega)} e^{2|k|r}. \tag{53}$$

The idea behind Calderón's method is to multiply (52) by a smooth cut-off function and then apply the inverse Fourier transform. Let $\hat{\eta} \in C_0^\infty(\mathbb{R}^2)$ be a nonnegative function supported in the unit ball with $\hat{\eta} = 1$ near $x = 0$, and let σ be a positive parameter determining the cut-off radius. Then from (52) we obtain

$$\mathcal{F}(\chi_\Omega(\gamma - 1))(-2k_1, 2k_2)\hat{\eta}\left(\frac{k}{\sigma}\right) = -\frac{\mathbf{t}^{\exp}(k)}{4\pi|k|^2}\hat{\eta}(k/\sigma) - R(k)\hat{\eta}\left(\frac{k}{\sigma}\right).$$

Changing variables $s = (s_1, s_2) = 2(-k_1, k_2)$ gives

$$\begin{aligned} &\mathcal{F}(\chi_\Omega(\gamma - 1))(s_1, s_2)\hat{\eta}\left(\frac{(-s_1, s_2)}{(2\sigma)}\right) \\ &= -\frac{\mathbf{t}^{\exp}((-s_1, s_2)/2)}{\pi|s|^2}\hat{\eta}\left(\frac{(-s_1, s_2)}{(2\sigma)}\right) - R\left(\frac{(-s_1, s_2)}{2}\right)\hat{\eta}\left(\frac{(-s_1, s_2)}{(2\sigma)}\right). \end{aligned} \tag{54}$$

Inverting $\mathcal{F}$ and neglecting the second term in (54) yields an approximation to γ:

$$\gamma^{\text{app}}(x) - 1 = -\frac{1}{2\pi}\int_{\mathbb{R}^2} e^{ix\cdot s}\frac{\mathbf{t}^{\exp}((-s_1, s_2)/2)}{\pi|s|^2}\hat{\eta}\left(\frac{(-s_1, s_2)}{(2\sigma)}\right)ds_1 ds_2.$$

Changing back the variables in the integral to $(k_1, k_2) = (-s_1, s_2)/2$ yields the formula

$$\begin{aligned}\gamma^{\text{app}}(x) - 1 &= -\frac{1}{2\pi^2}\int_{\mathbb{R}^2} e^{2i(-x_1k_1+x_2k_2)}\frac{\mathbf{t}^{\exp}(k)}{4|k|^2}\hat{\eta}\left(\frac{k}{\sigma}\right)4dk_1dk_2 \\ &= -\frac{2}{(2\pi)^2}\int_{\mathbb{R}^2} e_{-x}(k)\frac{\mathbf{t}^{\exp}(k)}{|k|^2}\hat{\eta}\left(\frac{k}{\sigma}\right)dk_1dk_2. \qquad (55)\end{aligned}$$

The reconstruction γ^{app} is an approximation of a low-pass filtered version of γ. Choosing the parameter σ as in [7] with $0 < \alpha < 1$ to be

$$\sigma = \frac{1-\alpha}{2r}\log\frac{1}{\|\gamma - 1\|_{L^\infty(\Omega)}} \qquad (56)$$

yields due to (53) the error estimate

$$\|\gamma^{\text{app}}(x) - \eta_\sigma * \gamma\|_{L^\infty} \le \|R(k)\hat{\eta}(k/\sigma)\|_{L^1(\mathbb{R}^2)} \le C\|\gamma - 1\|^{1+\alpha}_{L^\infty(\Omega)}(\log(\|\gamma - 1\|_{L^\infty(\Omega)}))^2.$$

Note that when $\|\gamma - 1\|_{L^\infty(\Omega)}$ is sufficiently small this error is much smaller than $\|\gamma - 1\|_{L^\infty(\Omega)}$. Since in most applications the approximate magnitudes of the conductivities comprising $\gamma(x)$ are known, an estimate to σ in (56) can be computed.

In summary, the algorithm proposed in [7] is tantamount to the following:

1. Compute $\mathbf{t}^{\exp}(k)$ by (4).
2. Construct a low-pass filter $\hat{\eta}(k/\sigma)$.
3. Compute the approximation γ^{app} by (55).

6.2. Calderón's method as an approximation of the D-bar method. Calderón's method using (55) can be seen as a three-step approximation of the D-bar method using (3) and (12)–(13):

1. In (12), $\mathbf{t}(k)$ is approximated by $\mathbf{t}^{\exp}(k)\hat{\eta}(k/\sigma)$, where $\hat{\eta}(k/\sigma)$ is a smooth cut-off function.
2. The function μ in the integral in the right-hand side of (12) is approximated by its asymptotic value $\mu \sim 1$.
3. The square function in (13) is linearized: $(1-h)^2 \sim 1 - 2h$.

In contrast, the D-bar method using $\mathbf{t}^{\exp}_{\text{R}}$ makes only the first approximation (with sharp cut-off).

7. Analysis of a simple radial conductivity distribution. In this section, we consider the simple example of a piecewise constant radial conductivity defined in the unit disc Ω. We will show that in this case $\mathbf{t}^{\exp}$ can be expanded conveniently using Bessel functions. Furthermore, such an expansion leads to a result concerning the asymptotic behavior of $\mathbf{t}^{\exp}(k)$ as $|k|$ tends to infinity. We will write out explicit formulas for γ^{app}, the Calderón reconstruction, and $\gamma^{\exp}$, the D-bar reconstruction of γ with the $\mathbf{t}^{\exp}$ approximation.

Consider the radial conductivity

$$\gamma(x) = \begin{cases} \sigma & \text{for } |x| \le r, \\ 1 & \text{for } |x| > r, \end{cases} \qquad (57)$$

where $0 < r < 1$ and $\sigma > 0, \sigma \ne 1$. Define

$$\alpha = \frac{\sigma - 1}{\sigma + 1}. \qquad (58)$$

According to [32], trigonometric basis functions are eigenfunctions for Λ_γ when γ is radial. More precisely, $\Lambda_\gamma \varphi_n = \lambda_n \varphi_n$ with $\varphi_n(\alpha) := (2\pi)^{-1/2} e^{in\alpha}$ for $n \in \mathbb{Z}$. It is well known [12] that the eigenvalues of Λ_γ corresponding to (57) are given by

$$\lambda_n = n\left(1 + \frac{2\alpha r^{2n}}{1-\alpha r^{2n}}\right), \quad n = 1, 2, 3, \ldots. \tag{59}$$

Hence $\delta\Lambda \equiv \Lambda_\gamma - \Lambda_1$ has eigenvalues

$$\delta\lambda_n = \frac{2n\alpha r^{2n}}{1-\alpha r^{2n}}, \quad n = 1, 2, 3, \ldots. \tag{60}$$

As in [29], one can derive a series representation of $\mathbf{t}^{\exp}(k)$. For the case of the conductivity distribution (57), this leads to a particularly simple representation of $\mathbf{t}^{\exp}$ in terms of Bessel functions, which we derive here. Expanding e^{ikx} in a Fourier series on the circle $x = e^{i\theta}$ yields [13]

$$e^{ikx} = \sum_{n=-\infty}^{\infty} a_n(k) e^{in\theta} \quad \text{with} \quad a_n(k) = \begin{cases} \frac{(ik)^n}{n!}, & n \geq 0, \\ 0, & n < 0. \end{cases}$$

Substituting this series into formula (4) and using (59) gives a series for $\mathbf{t}^{\exp}(k)$:

$$\mathbf{t}^{\exp}(k) = 2\pi \sum_{n=1}^{\infty} (\lambda_n - n) \frac{(-1)^n |k|^{2n}}{(n!)^2} = 4\pi\alpha \sum_{n=1}^{\infty} \frac{n r^{2n}}{1-\alpha r^{2n}} \frac{(-1)^n |k|^{2n}}{(n!)^2}. \tag{61}$$

Write $(1-\alpha r^{2n})^{-1} = \sum_{m=0}^{\infty} (\alpha r^{2n})^m$ so that

$$\mathbf{t}^{\exp}(k) = 4\pi\alpha \sum_{m=0}^{\infty} \alpha^m \sum_{n=1}^{\infty} \frac{n(-1)^n}{(n!)^2} (|k| r^{m+1})^{2n}. \tag{62}$$

Note that the Bessel function $J_1(t) = -J_0'(t) = -(2/t) \sum_{j=1}^{\infty} j(-1)^j (j!)^{-2} (t/2)^{2j}$. Thus, with $t = 2r^{m+1}|k|$,

$$\mathbf{t}^{\exp}(k) = -4\pi\alpha |k| r \sum_{m=0}^{\infty} (\alpha r)^m J_1(2r^{m+1}|k|). \tag{63}$$

This formula gives an accurate way for computing $\mathbf{t}^{\exp}$ numerically. Furthermore, we can derive the asymptotic behavior of $\mathbf{t}^{\exp}$ from (63).

For small z, $J_1(z) \sim z/2$. So using $\sum_{m=0}^{\infty} (\alpha r^2)^m = 1/(1-\alpha r^2)$ yields

$$\mathbf{t}^{\exp}(k) \sim -4\pi\alpha |k|^2 r \sum_{m=0}^{\infty} \alpha^m r^{2m+1} = \frac{-4\pi\alpha (|k| r)^2}{1-\alpha r^2} = O(|k|^2) \quad \text{for small } |k|.$$

For large $|z|$, we have $J_1(z) \sim (2/(\pi z))^{1/2} \cos(z - 3\pi/4) + e^{|\mathrm{Im}\, z|} O(1/|z|)$, and so

$$\mathbf{t}^{\exp}(k) \sim -4\pi\alpha |k| r \sum_{m=0}^{\infty} (\alpha r)^m \sqrt{\frac{1}{\pi r^{m+1} |k|}} \cos\left(2r^{m+1}|k| - \frac{3\pi}{4}\right)$$

for large $|k|$. After some simplification, this results in the asymptotic formula

$$\mathbf{t}^{\exp}(k) \sim \frac{-4\pi\alpha |k|^{1/2} r^{1/2}}{\sqrt{\pi}} \sum_{m=0}^{\infty} (\alpha)^m r^{m/2} \cos\left(2r^{m+1}|k| - \frac{3\pi}{4}\right) = O(|k|^{1/2}). \tag{64}$$

Note that (64) shows the importance of truncation of $\mathbf{t}^{\exp}$: the solvability of the D-bar equation is not proven for $\mathbf{t}^{\exp}$ with asymptotic behavior (64).

7.1. Calderón's method for a simple radial conductivity. Let γ be of the form (57). Note from [14], for example, that the Fourier transform of the characteristic function χ_r is given by

$$\begin{aligned}\mathcal{F}^{-1}(\chi_r)(k) = \check{\chi}_r(k) &= \frac{1}{2\pi}\int_{\mathbb{R}^2}\chi_r(p)e^{ik\cdot p}dp = \frac{1}{2\pi}\int_0^r\int_0^{2\pi} e^{i|k|\rho\cos(\theta)}\rho d\rho d\theta\\ &= \frac{1}{2\pi}\sum_{j=0}^{\infty}\frac{(i|k|)^j}{j!}\int_0^r\rho^{j+1}d\rho\int_0^{2\pi}\cos^j(\theta)d\theta\\ &= \begin{cases}\sum_{j=0}^{\infty}\frac{(i|k|)^j}{j!}\frac{r^{j+2}}{j+2}\frac{1\cdot3\cdot5\cdots(j-1)}{2\cdot4\cdot6\cdots j}, & j \text{ even},\\ 0, & j \text{ odd}\end{cases}\\ &= \sum_{m=0}^{\infty}\frac{(m+1)(-1)^m}{((m+1)!)^2}\left(\frac{r|k|}{2}\right)^{2m}\frac{r^2}{2}\\ &= -\frac{2}{|k|^2}\sum_{n=1}^{\infty}\frac{n(-1)^n}{(n!)^2}\left(\frac{r|k|}{2}\right)^{2n}.\end{aligned}$$

Thus, from (62),

$$\mathbf{t}^{\exp}(k) = -8\pi|k|^2\alpha\sum_{m=0}^{\infty}\alpha^m\check{\chi}_{r^{m+1}}(2k). \tag{65}$$

For this simple case, we can substitute $\mathbf{t}^{\exp}$ directly into (55) and compute explicitly without multiplying by the cut-off function $\hat{\eta}$ (or, equivalently, take $\sigma=\infty$, implying $\hat{\eta}\equiv 1$). Thus Calderón's reconstruction γ^{app} is given by

$$\begin{aligned}\gamma^{\text{app}}(x) &= 1 - \frac{8}{(2\pi)^2}\int_{\mathbb{R}^2}e_{-x}(k)\frac{\mathbf{t}^{\exp}(k)}{|k|^2}dk_1dk_2\\ &= 1 + \frac{4}{\pi}\int_{\mathbb{R}^2}e_{-x}(k)\alpha\sum_{m=0}^{\infty}\alpha^m\check{\chi}_{r^{m+1}}(2|k|)dk_1dk_2\\ &= 1 + 2\alpha\sum_{m=0}^{\infty}\alpha^m\frac{1}{2\pi}\int_{\mathbb{R}^2}e^{-i(x_1w_1-x_2w_2)}\check{\chi}_{r^{m+1}}(|w|)dw_1dw_2\\ &= 1 + 2\alpha\sum_{m=0}^{\infty}\alpha^m\frac{1}{2\pi}\int_{\mathbb{R}^2}e^{-ix\cdot\bar{w}}\check{\chi}_{r^{m+1}}(|w|)dw_1dw_2\\ &= 1 + 2\alpha\sum_{m=0}^{\infty}\alpha^m\mathcal{F}(\check{\chi}_{r^{m+1}}(|s|)) \qquad (66)\\ &= 1 + 2\alpha\sum_{m=0}^{\infty}\alpha^m\chi_{r^{m+1}}(x). \qquad (67)\end{aligned}$$

Note that (67) preserves the location of the jump in the actual conductivity distribution γ. Furthermore, elementary calculations show $\gamma^{\text{app}}(0)=\sigma$; i.e., the correct value of the conductivity is attained at $x=0$.

Similar computations were done in [14] (see also [13]), where the starting point, however, was the Neumann-to-Dirichlet (ND) map. They found the approximation

$$\gamma(x) \approx 1 + 2\alpha\sum_{m=0}^{\infty}(-\alpha)^m\chi_{r^{m+1}}(x). \tag{68}$$

7.2. The D-bar method for a simple radial conductivity. The series (65) can be used in the analysis of the truncated D-bar method. We have

$$\begin{aligned}
\gamma_{\mathrm{R}}^{\exp}(x)^{1/2} \equiv \mu_{\mathrm{R}}^{\exp}(x,0) &= 1 - \frac{1}{4\pi^2}\int_{\mathbb{R}^2} \frac{\mathbf{t}^{\exp}(k)}{|k|^2} e_{-x}(k)\chi_R(|k|)\overline{\mu_{\mathrm{R}}^{\exp}(x,k)}dk_1dk_2 \\
&= 1 + \frac{2\alpha}{\pi}\sum_{m=0}^{\infty}\alpha^m \int_{\mathbb{R}^2} \check{\chi}_{r^{m+1}}(2|k|)e_{-x}(k)\chi_R(|k|)\overline{\mu_{\mathrm{R}}^{\exp}(x,k)}dk_1dk_2 \\
&= 1 + \frac{\alpha}{2\pi}\sum_{m=0}^{\infty}\alpha^m \int_{\mathbb{R}^2} \check{\chi}_{r^{m+1}}(|w|)e^{-ix\cdot\overline{w}}\chi_R(2|w|)\overline{\mu_{\mathrm{R}}^{\exp}\left(x,\frac{w}{2}\right)}dw_1dw_2 \\
&= 1 + \frac{\alpha}{2\pi}\sum_{m=0}^{\infty}\alpha^m \int_{\mathbb{R}^2} \check{\chi}_{r^{m+1}}(|s|)e^{-ix\cdot s}\chi_R(2|s|)\overline{\mu_{\mathrm{R}}^{\exp}\left(x,\frac{\overline{s}}{2}\right)}ds_1ds_2 \\
&= 1 + \alpha\sum_{m=0}^{\infty}\alpha^m \mathcal{F}\left(\check{\chi}_{r^{m+1}}(|\cdot|)\chi_R(2\cdot)\overline{\mu_{\mathrm{R}}^{\exp}\left(x,\frac{\cdot}{2}\right)}\right)(x) \\
&= 1 + \frac{\alpha}{2\pi}\sum_{m=0}^{\infty}\alpha^m \left(\chi_{r^{m+1}}(\cdot) * \mathcal{F}\left(\chi_R(2\cdot)\overline{\mu_{\mathrm{R}}^{\exp}\left(x,\frac{\cdot}{2}\right)}\right)\right)(x). \qquad (69)
\end{aligned}$$

It is evident from this formula that a ringing effect will appear in the reconstruction, but the effect will be somewhat blurred by the convolution of the characteristic functions with the Fourier transform of $\overline{\mu^{\exp}}$.

8. Numerical experiments. In this section, numerical examples are computed that offer intuition and illustrate the results of the previous sections.

8.1. Example conductivities. We consider discontinuous conductivities defined by (57) with all nine possible combinations of the choices $r \in \{0.2, 0.55, 0.9\}$ and $\sigma \in \{1.1, 2, 8\}$. See Figure 8.2 for profiles of the conductivities.

Radially symmetric examples are chosen for their ease of computation and display (it is sufficient to display profiles of the reconstructed conductivities and scattering transforms, which are real-valued and radially symmetric for radially symmetric examples), as well as to illustrate the results of sections 6 and 7.1. However, all of our computational methods apply equally well to nonsymmetric conductivities.

8.2. Results. The computed scattering transform is denoted by $\mathbf{t}_R^{\exp}$, where R indicates the truncation radius. We compute $\mathbf{t}_R^{\exp}$ from the Bessel-series formula (63) with 10 terms in the expansion, which was verified to be in very good agreement with computations of (61) with 45 eigenvalues. Figure 8.1 contains plots of the approximate scattering transforms $\mathbf{t}_R^{\exp}$ with constant multiples of $\sqrt{|k|}$ superimposed to illustrate the growth of $\mathbf{t}^{\exp}(k)$ as demonstrated in (64).

Plots of the reconstructed conductivities are found in Figures 8.2, 8.3, 8.4, and 8.5. Figure 8.2 contains plots of the reconstructed conductivities from the approximate scattering transform $\mathbf{t}_R^{\exp}$ with truncation radius $R = 15$ for rows 1 and 2 and $R = 12$ for row 3. Figure 8.3 illustrates the dependence of the reconstructions $\gamma_{\mathrm{R}}^{\exp}$ on R. Profiles of the reconstructed discontinuous conductivities with contrast 0.1 and a jump at $|x| = 0.2, 0.55$, and 0.9 are plotted for $R = 4, 5, 6, 7, 8$, and 15. The reconstructions from Calderón's linearization method are found in Figure 8.4. Finally, 2-D plots of three conductivities are included in Figure 8.5.

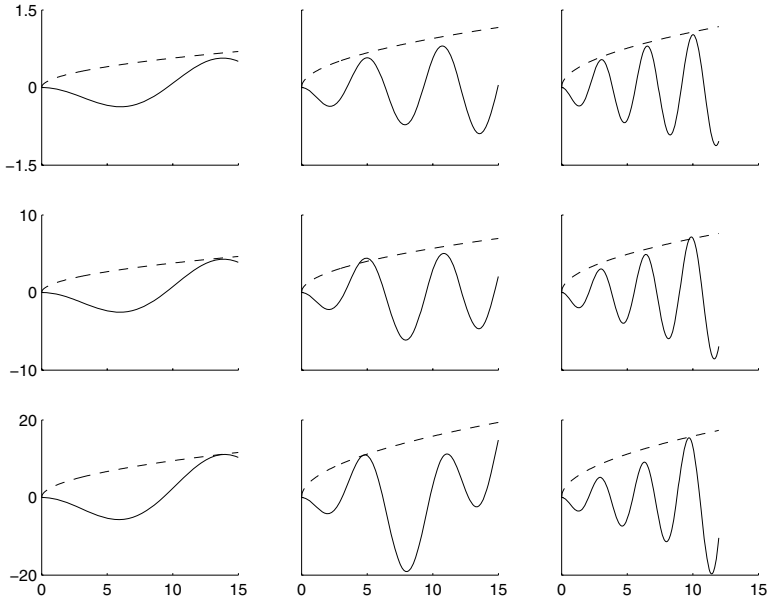

FIG. 8.1. *Profiles of approximate scattering transforms* $\mathbf{t}^{\exp}$ *(solid) for the discontinuous conductivity distributions given by* (57) *with constant multiples of* $\sqrt{|k|}$ *superimposed (dashed) to illustrate the growth of* $\mathbf{t}^{\exp}$*. The top row corresponds to* $\sigma = 1.1$ *in* (57)*, the middle row to* $\sigma = 2.0$*, and the bottom row to* $\sigma = 8.0$*. The first column corresponds to* $r = 0.2$ *in* (57)*, the second column to* $r = 0.55$*, and the third column to* $r = 0.9$*. Note that the vertical axis limits are the same in each row of plots.*

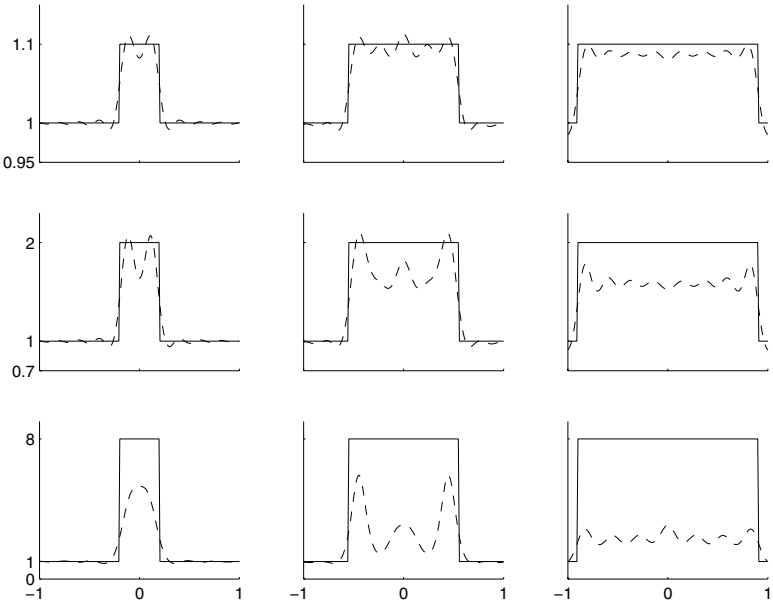

FIG. 8.2. *Actual (solid) and reconstructed (dashed) conductivity profiles* $\gamma_R^{\exp}$ *(*$R = 15$ *for the first two rows,* $R = 12$ *for the last row) for the discontinuous examples. Note that the vertical axis limits are the same in each row of plots.*

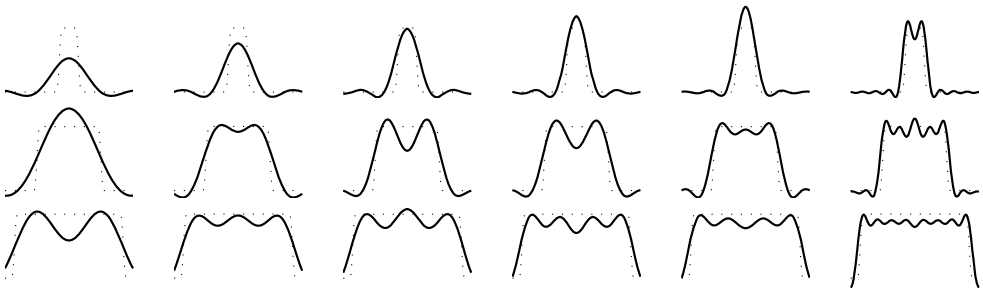

FIG. 8.3. *The discontinuous conductivity distributions (dotted lines) with a jump of* 0.1 *at* $|x| = 0.2$ *(top row),* 0.55 *(center row), and* 0.9 *(bottom row) reconstructed (solid line) from* $\mathbf{t}_R^{\exp}$ *with truncation radii* $R = 4, 5, 6, 7, 8, 15$ *(left to right). Note that the vertical axis limits are the same in each row of plots.*

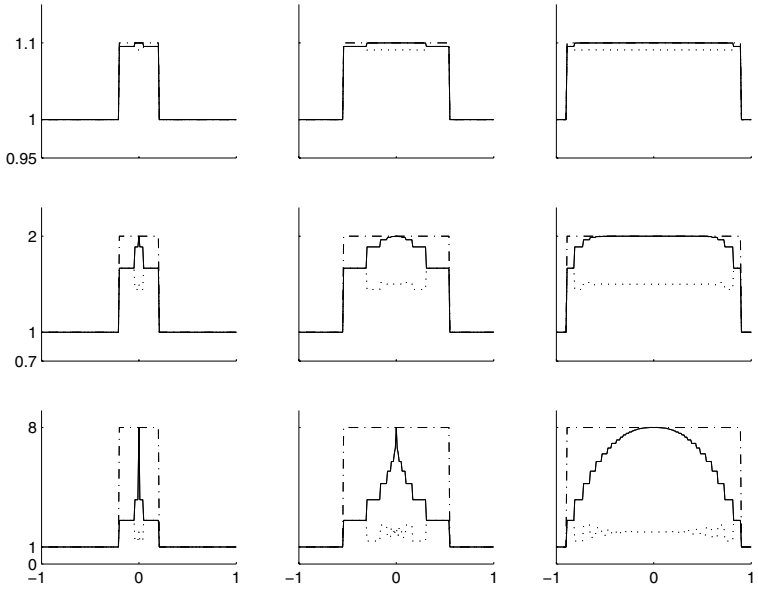

FIG. 8.4. *Actual (dash-dotted) and reconstructed conductivity profiles for the discontinuous examples. The dotted reconstructions are from Calderón's linearization formula* (68) *from the ND map, and the solid reconstructions are from Calderón's linearization formula* (67) *from the DN map. Note that the vertical axis limits are the same in each row of plots.*

8.3. Discussion. From Figure 8.1, we see that the scattering transforms demonstrate the expected asymptotic growth $\mathbf{t}^{\exp} \sim O(|k|^{1/2})$. The magnitude of the scattering transform increases with the amplitude of γ, and $\mathbf{t}^{\exp}$ becomes more oscillatory as $\operatorname{supp}(\gamma - 1)$ increases. This implies that conductivity distributions with high contrast near the boundary should be particularly difficult to reconstruct, because such a scattering transform is more sensitive to errors in $\partial\Lambda_\gamma$ and more difficult to represent on a discrete mesh.

We see from the corresponding reconstructions in Figure 8.2 that in all cases the location of the jump is reconstructed equally well, but a loss in accuracy in the amplitude becomes apparent as the contrast increases and as the support of $\gamma -$

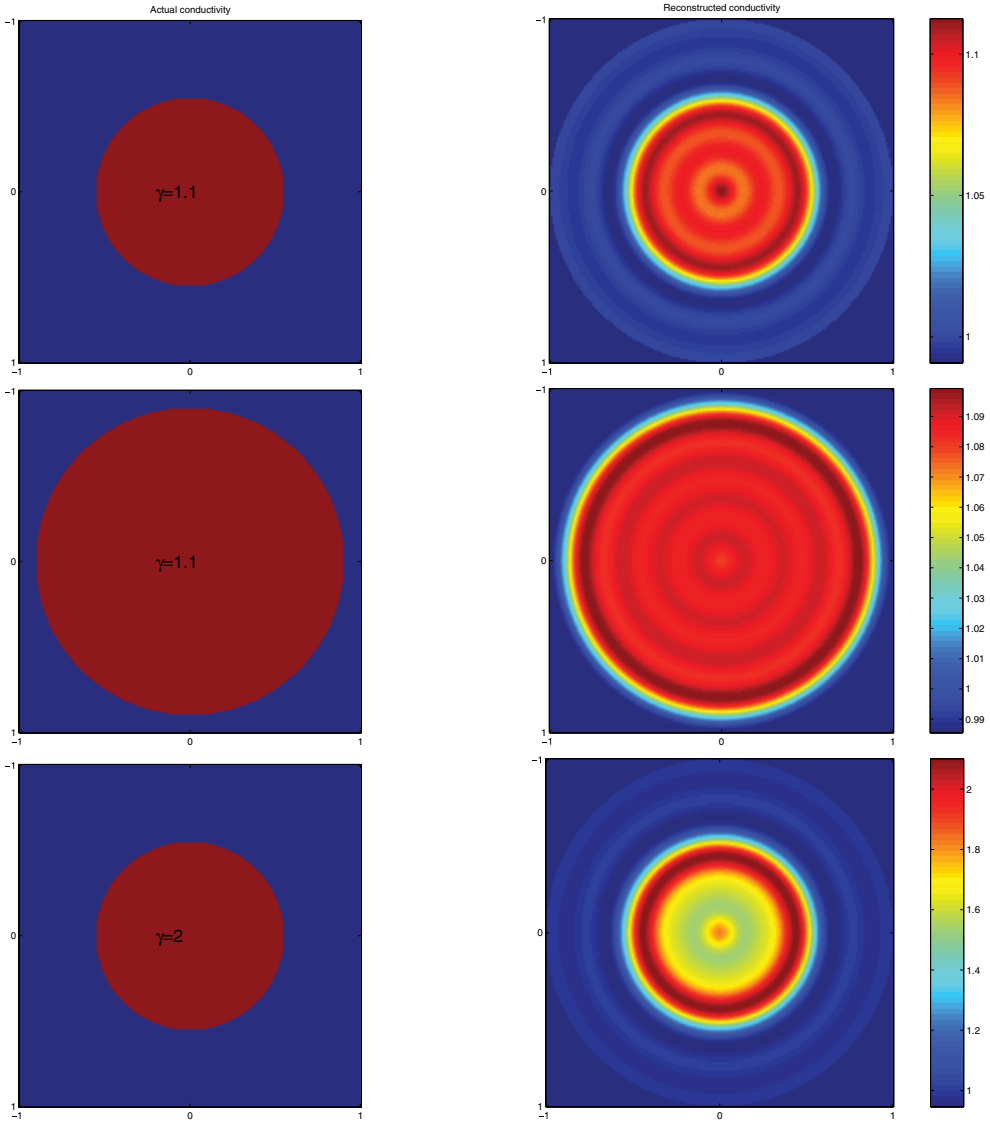

FIG. 8.5. *Three discontinuous conductivity distributions (left) reconstructed (right) from* $\mathbf{t}_R^{\exp}$ *with truncation radius* $R = 15$.

1 widens. This corresponds to the fact that the approximation $\psi|_{\partial\Omega} = e^{izk}|_{\partial\Omega}$ is better the smaller the contrast and the smaller the support of $\gamma - 1$. We see that the reconstructions tend to underestimate the actual amplitude of the conductivity more markedly as the support of $\gamma - 1$ widens and as the magnitude of γ increases. Also note that the reconstructions of the discontinuous conductivities are smooth, as predicted by Proposition 3.5. In Figure 8.3, the nature of the dependence of the smooth approximations on R can be observed. A Gibbs-type phenomenon is indeed present, as suggested by formula (69). Also, the support of $\gamma - 1$ is reconstructed with reasonable accuracy even for very small truncation radii, while the general shape and amplitude of γ is reconstructed with increasing accuracy as R increases. Thus, in

practice one should choose R as large as possible before blow-up of $\mathbf{t}^{\exp}$ is evident. In [29, 24, 15, 16], R was chosen by inspection.

The reconstructions from Calderón's linearization method are found in Figure 8.4. It is interesting to note that the linearized reconstruction from the DN map (67) achieves a more accurate approximation to the amplitude of the conductivity than the linearized reconstruction from the ND map (68). This result also holds for conductivities whose jump is negative ($0 < \sigma < 1$) in $|x| < r$. Note that the linearization formula (67) actually achieves the amplitude of the actual conductivity (albeit only at a single point in some cases), while the D-bar reconstruction $\gamma^{\exp}$ does not. This is presumably due to the damping effect of the convolution with the Fourier transform of $\overline{\mu^{\exp}}$ in (69).

Finally, in Figure 8.5 we display three reconstructions in the typical 2-D display mode for reconstructions from experimental data. This figure further illustrates the ringing effect in the reconstructions of the discontinuous conductivities.

Acknowledgments. The authors thank David Isaacson for helpful discussions and the anonymous reviewers for their suggestions.

REFERENCES

[1] M. B. P. Amato, C. S. Barbas, D. M. Medeiros, R. B. Magaldi, G. P. Schettino, G. Lorenzi-Filho, R. A. Kairalla, D. Deheinzelin, C. Morais, E. O. Fernandes, T. Y. Takagaki, and C. R. R. Carvalho, *Effect of a protective-ventilation strategy on mortality in the acute respiratory distress syndrome*, New England J. Med., 338 (1998), pp. 347–354.

[2] K. Astala and L. Päivärinta, *Calderón's inverse conductivity problem in the plane*, Ann. of Math. (2), 163 (2006), pp. 265–299.

[3] K. Astala, M. Lassas, and L. Päivärinta, *Calderón's inverse problem for anisotropic conductivity in the plane*, Comm. Partial Differential Equations, 30 (2005), pp. 207–224.

[4] J. A. Barceló, T. Barceló, and A. Ruiz, *Stability of the inverse conductivity problem in the plane for less regular conductivities*, J. Differential Equations, 173 (2001), pp. 231–270.

[5] L. Borcea, *Electrical impedance tomography*, Inverse Problems, 18 (2002), pp. 99–136.

[6] R. M. Brown and G. Uhlmann, *Uniqueness in the inverse conductivity problem for nonsmooth conductivities in two dimensions*, Comm. Partial Differential Equations, 22 (1997), pp. 1009–1027.

[7] A. P. Calderón, *On an inverse boundary value problem*, in Seminar on Numerical Analysis and its Applications to Continuum Physics, Sociedade Brasileira de Matemática, Rio de Janeiro, Brazil, 1980, pp. 65–73.

[8] M. Cheney, D. Isaacson, and J. C. Newell, *Electrical impedance tomography*, SIAM Rev., 41 (1999), pp. 85–101.

[9] W. Daily and A. L. Ramirez, *Electrical imaging of engineered hydraulic barriers*, Geophysics, 65 (2000), pp. 83–94.

[10] W. Daily, A. Ramirez, and R. Johnson, *Electrical impedance tomography of a perchloroethylene release*, J. Environ. Eng. Geophys., 2 (1998), pp. 189–201.

[11] M. R. Eggleston, R. J. Schwabe, D. Isaacson, and L. F. Coffin, *The application of electric current computed tomography to defect imaging in metals*, in Review of Progress in Quantitative NDE, Vol. 9A, Plenum Press, New York, 1990, pp. 455–462.

[12] D. G. Gisser, D. Isaacson, and J. C. Newell, *Electric current computed tomography and eigenvalues*, SIAM J. Appl. Math., 50 (1990), pp. 1623–1634.

[13] D. Isaacson and M. Cheney, *Effects of measurement precision and finite numbers of electrodes on linear impedance imaging algorithms*, SIAM J. Appl. Math., 51 (1989), pp. 1705–1731.

[14] D. Isaacson and E. L. Isaacson, *Comment on Calderón's paper: "On an inverse boundary value problem,"* Math. Comp., 52 (1989), pp. 553–559.

[15] D. Isaacson, J. L. Mueller, J. C. Newell, and S. Siltanen, *Reconstructions of chest phantoms by the D-bar method for electrical impedance tomography*, IEEE Trans. Med. Imaging, 23 (2004) pp. 821–828.

[16] D. Isaacson, J. L. Mueller, J. C. Newell, and S. Siltanen, *Imaging cardiac activity by the D-bar method for electrical impedance tomography*, Physiol. Meas., 27 (2006), pp. S43–S50.

[17] A. Kemna, A. Binley, A. Ramirez, and W. Daily, *Complex resistivity tomography for environmental applications*, Chem. Eng. J., 77 (2000), pp. 11–18.
[18] K. Knudsen, *On the Inverse Conductivity Problem,* Ph.D. thesis, Department of Mathematical Sciences, Aalborg University, Aalborg, Denmark, 2002.
[19] K. Knudsen, *A new direct method for reconstructing isotropic conductivities in the plane,* Physiol. Meas., 24 (2003), pp. 391–401.
[20] K. Knudsen and A. Tamasan, *Reconstruction of less regular conductivities in the plane*, Comm. Partial Differential Equations, 29 (2004), pp. 361–381.
[21] K. Knudsen, J. L. Mueller, and S. Siltanen, *Numerical solution method for the D-bar equation in the plane*, J. Comput. Phys., 198 (2004), pp. 500–517.
[22] J. L. Lions and E. Magenes, *Nonhomogeneous Boundary Value Problems and Applications,* Vol. I, Springer-Verlag, New York, Heidelberg, 1972.
[23] L. Liu, *Stability Estimates for the Two-Dimensional Inverse Conductivity Problem*, Ph.D. thesis, University of Rochester, Rochester, NY, 1997.
[24] J. L. Mueller and S. Siltanen, *Direct reconstructions of conductivities from boundary measurements*, SIAM J. Sci. Comput., 24 (2003), pp. 1232–1266.
[25] A. I. Nachman, *Global uniqueness for a two-dimensional inverse boundary value problem*, Ann. of Math. (2), 143 (1996), pp. 71–96.
[26] A. I. Nachman, *Global Uniqueness for a Two-Dimensional Inverse Boundary Value Problem*, Preprint Series 19, Department of Mathematics, University of Rochester, Rochester, NY, 1993.
[27] A. L. Ramirez and W. Daily, *Electrical imaging at the large block test—Yucca Mountain, Nevada*, J. Appl. Geophys., 46 (2001), pp. 85–100.
[28] M. Reed and B. Simon, *Methods of Modern Mathematical Physics.* I: *Functional Analysis*, 2nd ed., Academic Press, New York, 1980.
[29] S. Siltanen, J. Mueller, and D. Isaacson, *An implementation of the reconstruction algorithm of A. Nachman for the* 2*-D inverse conductivity problem,* Inverse Problems, 16 (2000), pp. 681–699.
[30] L. Slater, A. M. Binley, W. Daily, and R. Johnson, *Cross-hole electrical imaging of a controlled saline tracer injection*, J. Appl. Geophys., 44 (2000), pp. 85–102.
[31] S. Stefanescu, C. Schlumberger, and M. Schlumberger, *Sur la distribution électrique potentielle autour d'une prise de terre ponctuelle dans un terrain à couches horizontales, homogènes et isotropes*, J. Physics and Radium Ser., 7 (1930), pp. 132–140.
[32] J. Sylvester, *A convergent layer stripping algorithm for the radially symmetric impedance tomography problem*, Comm. Partial Differential Equations, 17 (1992), pp. 1955–1994.
[33] M. E. Taylor, *Partial Differential Equations: Basic Theory*, Texts Appl. Math., 23, Springer-Verlag, New York, 1996.
[34] F. C. Trigo, R. Gonzalez-Lima, and M. B. P. Amato, *Electrical impedance tomography using the extended Kalman filter*, IEEE Trans. Biomed. Eng., 51 (2004), pp. 72–81.
[35] I. N. Vekua, *Generalized Analytic Functions*, Pergamon Press, London, Paris, Frankfurt, 1962.
[36] R. A. Williams and M. S. Beck, eds., *Process Tomography-Principles, Techniques, and Applications*, Butterworth-Heinemann, Oxford, UK, 1995.
[37] C. G. Xie, S. M. Huang, B. S. Hoyle, and M. S. Beck, *Tomographic imaging of industrial process equipment-development of system model and image reconstruction algorithm for capacitive tomography*, in Proceedings of the 5th Conference on Sensors and Their Applications, Edinburgh, Scotland, 1991, pp. 203–208.
[38] G. A. Uhlmann, *Developments in inverse problems since Calderón's foundational paper*, in Harmonic Analysis and Partial Differential Equations (Chicago, IL, 1996), University of Chicago Press, Chicago, IL, 1999.
[39] C. G. Xie, A. Plaskowski, and M. S. Beck, 8*-electrode capacitance system for two-component flow identification*, IEEE Proc. A, 136 (1989), pp. 173–190.